

Nonuniform temperature effects on the QCD phase transition

Jun-Hui Zheng and Lijia Jiang

Center for Quantum Spintronics, Department of Physics,
Norwegian University of Science and Technology, NO-7491 Trondheim, Norway

We study nonuniform temperature effects on the dynamical phase transition in the relativistic heavy-ion collision. We reveal that the dynamical phase transition generally happens before the quark-gluon-plasma cools down to the equilibrium phase transition temperature if the nonuniform temperature effects are dominant compared to the dynamical memory effects. The phase transition temperature can be about 7 MeV and 14 MeV ahead when the temperature gradient is set to be 20 MeV/fm and 40 MeV/fm, respectively. Both the fluctuation and the correlation length of the chiral order parameter are enhanced near the phase transition point, and they increase from the crossover regime to the first order phase transition regime without exotic behavior at the critical point. The correlation length in the critical point regime is estimated.

I. INTRODUCTION

Exploring the QCD phase boundary and critical point (CP) is one of the main goals in relativistic heavy-ion collision (RHIC) experiments [1–5]. In the collider, a fireball quickly forms and cools down continuously. During the expansion of the fireball, the QCD matter cools from the quark-gluon-plasma (QGP) phase to the hadronic phase. A dynamical phase transition (PT) surface exists in the fireball, which separates the two phases [6–10]. The hadrons and resonances outside the surface collide with each other and part of them decay. A hypersurface named chemical freeze-out surface subsequently coexists outside the dynamical PT surface, where the inelastic collision between the hadronic matter ceases [11].

Recent studies show that in the QCD phase diagram, the chemical freeze-out line determined by experimental measurements and the statistical model lies on the up boundary of the equilibrium PT band from the lattice calculations at baryon chemical potential $\mu \leq 300$ MeV [12–19]. Given the uncertainties from both experimental measurements and lattice calculations at large baryon chemical potentials, there is possibility that the dynamical PT inside the fireball happens at temperature above the equilibrium PT temperature (see the sketch of an instantaneous fireball in Fig. 1). This is in contrast to the dynamical delay effects in a temperature uniform system, where the dynamical PT follows and memorizes the behaviors of equilibrium PT [20–23].

In this paper, we pursue to discuss the relation between the dynamical and the equilibrium PT surface in the fireball, by studying the behaviors of the QCD order parameter field (i.e., the σ field) in spatially nonuniform temperature profiles near the dynamical PT surface. As both the position and the shape of the dynamical PT surface vary with time during the fireball evolution, we look into the σ field in the comoving frame of the PT region. As shown in Fig. 1, we take a instantaneous slender brick cell in the fireball with the dynamical and equilibrium phase boundary located in the middle. In this brick cell, the temperature is spatially nonuniform. We further suppose the relaxation of the σ field configurations in the brick cell at various time approaches to zero. Thus, the σ field reaches the thermal equilibrium distribution instantly. With this Markov assumption, the instantaneous dynamical PT surface turns into the stationary PT surface in a nonuniform tem-

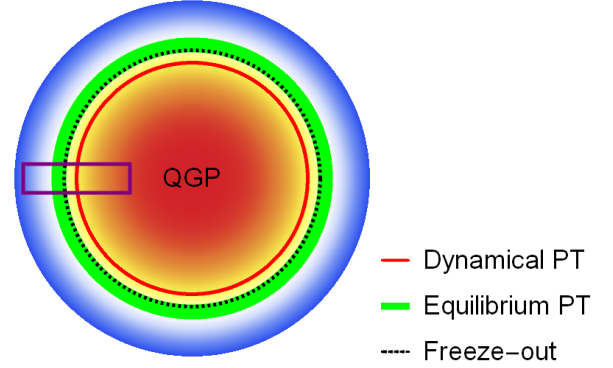


FIG. 1. A sketch of an instantaneous fireball. The temperature decreases from inner to outer (red to blue). The red solid circle represents the dynamical phase transition (PT) surface. The black dashed line is the freeze-out surface. The green brush line refers to the isothermal surface of the equilibrium PT temperature.

perature system.

We illustrate that the PT temperature in a temperature-nonuniform system is above the equilibrium PT temperature T_c of a temperature-uniform system. It means that hadrons form before the QGP cools down to T_c , if the spatially nonuniform temperature effects play a major role during the fireball evolution. We discuss the fluctuation strength and the correlation length of the σ field at the PT region, and find that the CP presents no typical critical behaviors compared to the other PT scenarios. At the same time, the correlation length in the PT region is significantly increased compared to that in the periphery of the cell.

II. TEMPERATURE PROFILE

First, we formalize the temperature profile in the brick cell. For simplicity, we suppose the y-z plane is isothermal, and the temperature function along the x-axis is spatially dependent,

$$T(x) = T_c + \frac{\delta T}{2} \tanh\left(\frac{x}{w}\right), \quad (1)$$

where δT is the temperature bias between the two ends of the cell and the width w dominates the range of the region near

the equilibrium PT surface where a finite temperature gradient ($\sim \delta T/2w$) presents. Note that the real temperature profile is determined by the background matter fields (hadrons, quarks and gluons) [24]. For simplicity, we also assume the baryon chemical potential is homogeneous in the cell, and focus mainly on the nonuniform temperature effects.

III. PARTITION FUNCTION

As the local equilibrium assumption in relativistic hydrodynamics is proved to be well-performed [24–29], we carry on this assumption in our calculation. Thus, the partition function of the system is a product of the local partition function of the σ field at different x . In the continuous limit, we have

$$\mathcal{Z}[\sigma] = \int \mathcal{D}\sigma P[\sigma], \quad (2)$$

where the weight function is

$$P[\sigma] = \exp \left\{ - \int d\mathbf{r} \frac{(\nabla\sigma)^2/2 + V[\sigma(\mathbf{r})]}{T(x)} \right\}, \quad (3)$$

with $\mathbf{r} = (x, y, z)$. The effective potential of the σ field can be obtained from the QCD-inspired models [17, 30–34]. As we mainly focus on the regime near the CP, we parameterize the potential by analogy to the Ising model. In the simplest Ising mapping [35–37], we have

$$V[\sigma] = a(T - T_c)(\sigma - \sigma_0) + b(\mu - \mu_c)(\sigma - \sigma_0)^2 + c(\sigma - \sigma_0)^4, \quad (4)$$

where $a > 0$, $b < 0$ and $c > 0$ are parameters which depend on the real effective potential, (μ_c, T_c) marks the position of the equilibrium CP. Note that within this mapping, the PT temperature is μ independent. For $\Delta\mu \equiv \mu - \mu_c > 0$ and $\Delta\mu < 0$, the effective potential describes a first order PT and crossover respectively as the change of temperature. σ_0 (about 45 MeV) is introduced to shift the σ field to the realistic values. Since the value of σ_0 will not influence our discussion on fluctuations and correlation length, we simply set $\sigma_0 = 0$ in the following. Then, in thermal equilibrium, $\sigma < 0$ and $\sigma > 0$ correspond to the QGP phase and the hadron phase, respectively.

Throughout the article, we set the parameters $a = 0.5 \text{ fm}^{-2}$, $b = -0.25 \text{ fm}^{-1}$, and $c = 3.6$, to simulate the effective potential from the linear sigma model [33, 34]. The PT temperature $T_c = 160 \text{ MeV}$ is chosen from the result of lattice simulations [17, 18]. For the temperature profile, the temperature bias is set as $\delta T = 40 \text{ MeV}$ and the width is set to be $w = 1 \text{ fm}$ (or $w = 0.5 \text{ fm}$). Then the temperature gradient is 20 MeV/fm (40 MeV/fm), corresponding to the mean temperature gradient in a fireball of radius 10 fm with central temperature 200 MeV (400 MeV).

IV. THE ORDER PARAMETER PROFILE

Since the temperature is spatially nonuniform, the local order parameter which maximizes the weight function is

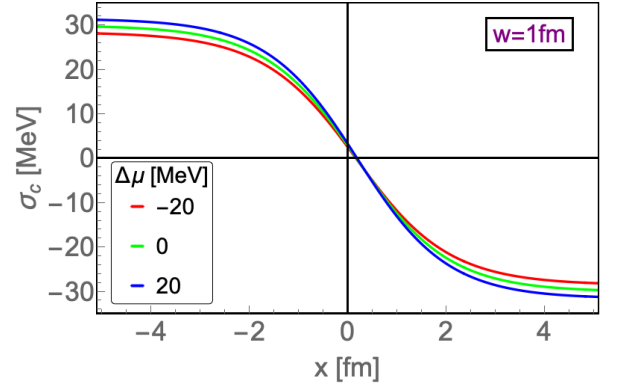


FIG. 2. The order parameter profile $\sigma_c(x)$ in the brick cell, with the red, green and blue lines represent results in the crossover ($\Delta\mu < 0$), CP ($\Delta\mu = 0$) and the first order PT ($\Delta\mu > 0$) scenarios, respectively.

never again determined by minimizing the effective potential $\partial V[\sigma]/\partial\sigma = 0$, but satisfies the extreme value condition of the weight function, $\delta P[\sigma]/\delta\sigma = 0$. Explicitly, we have

$$\nabla^2\sigma = \frac{1}{T}\nabla T \cdot \nabla\sigma + \frac{\delta V}{\delta\sigma}. \quad (5)$$

As we suppose the temperature distribution in the y - z plane is isothermal, the $\sigma(\mathbf{r})$ that maximizes the weight function must be flat in this plane. Thus $\sigma(\mathbf{r})$ depends only on x , and Eq.(5) reduces to a one-dimensional problem. The boundary condition is given by the local order parameters at infinite distance, i.e., $\sigma(x = -\infty) = \sigma_L$ and $\sigma(x = \infty) = \sigma_R$, where σ_L and σ_R are the minimum point of the potential $V[\sigma]$ at $x = \mp\infty$. Here, we have assumed that the cell's length is much larger than w .

The solution $\sigma_c(x)$ to Eq. (5) is presented in Fig. 2, with $w = 1 \text{ fm}$ and different $\Delta\mu$. A main information from these order parameter profiles is that $\sigma_c(x)$ changes its sign at $x > 0$, no matter the sign and magnitude of $\Delta\mu$. It is easy to check that, without the temperature gradient term $(1/T)\nabla T \cdot \nabla\sigma$, the solution $\sigma_c(x)$ is an odd function of x and vanishes at $x = 0$. As the $(1/T)\nabla T \cdot \nabla\sigma$ term is always negative ($\partial_x\sigma < 0$ and $\partial_x T > 0$), it will always contribute similar corrections to the solution $\sigma_c(x)$, and the sign change of $\sigma_c(x)$ will universally happens at $x > 0$. This result can be comprehended directly from the weight function Eq. (3). In the brick cell, the hot part with high temperature is more easily fluctuated than the cold part. Therefore, $\sigma_c(x)$ will tend to the order parameter value of the cold part, and $\sigma_c(0)$ becomes positive.

V. THERMAL FLUCTUATIONS

The fluctuations of the σ field are also changed by the temperature profile. We expand the σ field around the variational extremum solution with a small fluctuation, $\sigma(\mathbf{r}) = \sigma_c(x) + \delta\sigma(\mathbf{r})$. The weight function $P[\sigma]$ becomes

$$P[\sigma] = \exp \left[- \int d\mathbf{r} \frac{(\nabla\delta\sigma)^2/2 + m^2\delta\sigma^2/2 + 4c\sigma_c\delta\sigma^3 + c\delta\sigma^4}{T(x)} \right], \quad (6)$$

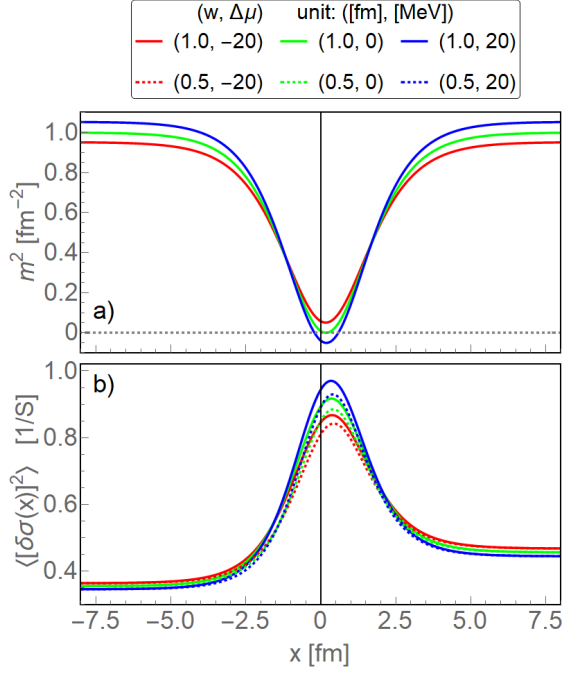


FIG. 3. Panel a) presents the local mass square of the fluctuating σ field, and panel b) presents the variance of the $\delta\sigma$ field, for different w and $\Delta\mu$. In both panels, the red, green and blue lines represents results in the crossover ($\Delta\mu < 0$), CP ($\Delta\mu = 0$) and the first order PT ($\Delta\mu > 0$) scenarios, respectively. Solid lines are results with $w = 1$ fm, and dotted lines are results with $w = 0.5$ fm.

where the mass term $m^2(x) = 2b\Delta\mu + 12c\sigma_c^2$ is spatially dependent. In the following, we mainly focus on the variance of the fluctuations, so we omit the cubic and quartic terms which are related to the higher order cumulants of fluctuations [38, 39].

Conventionally, we start the discussion from the mass term of the $\delta\sigma$ field. In a temperature-uniform system, the mass term relates to the correlation length: $\xi = 1/m$. In the nonuniform case, we follow the old way and define a local correlation length: $\xi_{local}(x) = 1/\sqrt{m^2(x)}$. We present the results of $m^2(x)$ in the brick cell in Fig. 3. In the periphery, $m^2 \approx 1 \text{ fm}^{-2}$ corresponds to $\xi_{local} \approx 1 \text{ fm}$, which is coincide with ξ since the temperature becomes flat apart from the center. In the central part, $m^2(x)$ presents exotic behaviors for different PT scenarios. In the crossover regime ($\Delta\mu < 0$), $m^2(x) > 0$ everywhere. For the critical value ($\Delta\mu = 0$), $m^2(x)$ vanishes at $\sigma_c = 0$, and the local correlation length ξ_{local} diverges. For the first order PT regime ($\Delta\mu > 0$), $m^2(x)$ can even be negative near the point $\sigma_c = 0$. Thus our definition of the local correlation length is not appropriate in the PT region with a finite temperature gradient. As we will show below, the variance of the local fluctuation $\delta\sigma(x)$ is always positive, and is better-suited to the description of the temperature nonuniform system.

We presume the size along the y and z direction is much smaller than the unknown correlation length, thus we adopt the zero-mode approximation for y and z directions, and $\delta\sigma(\mathbf{r})$ depends only on x . The cross-section of the brick cell is denoted as S . Discretizing the x -axis with spacing length Δx ,

the weight function becomes

$$P[\sigma] \approx \exp \left\{ -\frac{S}{2} \sum_{i,j} \delta\sigma_i M_{ij} \delta\sigma_j \right\}, \quad (7)$$

where the nonzero elements of the matrix M are

$$M_{ii} = \frac{1}{\Delta x} \left[\frac{1}{T_{i-1/2}} + \frac{1}{T_{i+1/2}} \right] + \frac{m_i^2 \Delta x}{T_i}, \quad (8)$$

$$M_{i,i+1} = M_{i+1,i} = -\frac{1}{T_{i+1/2} \Delta x}. \quad (9)$$

Here, ‘ i ’ refers to the position $x = i\Delta x$. The matrix M must be positive definite so that the solution σ_c maximizes the weight function. We would like to emphasize the necessity and importance of the kinetic energy in M , which is finite and solves the negative $m^2(x)$ problem in the first order PT scenario. This is because $m^2(x)$ constructs a well potential as shown in Fig. 3, and the kinetic term has to be finite due to the uncertainty principle. From the same reason, at $\Delta\mu = 0$, the fluctuations on the CP is not divergent due to a positive ground energy of M . The nonzero-mode fluctuation of the σ -field along x -direction plays a crucial role.

The variance of the local fluctuations is

$$\langle [\delta\sigma_i]^2 \rangle = \frac{[M^{-1}]_{ii}}{S}. \quad (10)$$

In Fig. 3, we plot the results of the variance for different w and $\Delta\mu$. We identify the maximum point of the variance as the PT point as usual. Note that the PT point locates a little right of the minimum point of $m^2(x)$, because the fluctuations in the right of the cell is lifted due to a higher temperature compared to the left. So the PT point always locates at $x > 0$ and the corresponding PT temperature is generally higher than T_c . The fluctuations near the PT point is finite and is significantly larger than those regions apart from the transition point. Interestingly, the fluctuations on the PT point monotonically increase from the crossover ($\Delta\mu < 0$) to the first order PT ($\Delta\mu > 0$). There are no exotic behaviors to characterize the CP ($\Delta\mu = 0$). In addition, the fluctuations near the PT point are enhanced as the increase of the width w for all the three scenarios. This can be easily understood in the extreme case that $w \rightarrow \infty$, the temperature becomes flat locally and the fluctuations near the CP become divergent.

The PT temperature can be evaluated from the temperature profile at the maximum point of the variance. In Fig. 4, we show the PT temperature for the two widths $w = 1 \text{ fm}$ and $w = 0.5 \text{ fm}$. The PT temperature is lifted about 7 MeV and 14 MeV, respectively, comparing with the equilibrium T_c . Remarkably, the spatial distribution of temperature leads to an early PT ahead of the equilibrium T_c , and a steeper change of the temperature distribution will lead to a higher PT temperature.

We further calculate the correlation length from the normalized nonlocal correlation in the brick cell,

$$G(x) = \frac{\langle \delta\sigma(x_p + x/2) \delta\sigma(x_p - x/2) \rangle}{\langle \delta\sigma(x_p) \delta\sigma(x_p) \rangle}, \quad (11)$$

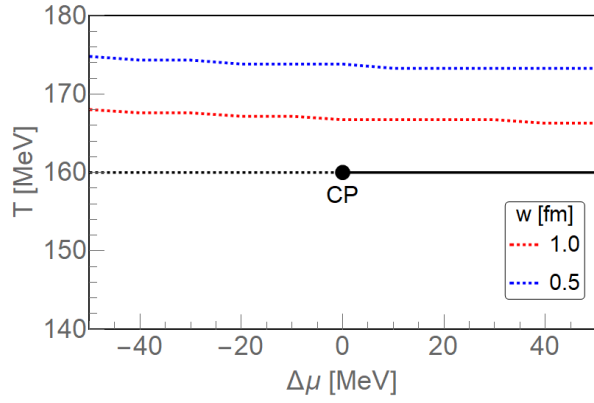


FIG. 4. A comparison of the PT temperature in the temperature-nonuniform (red and blue dotted lines) and temperature-uniform systems (black lines). The red dotted line is with $w = 1.0$ fm, and the blue dotted line is with $w = 0.5$ fm.

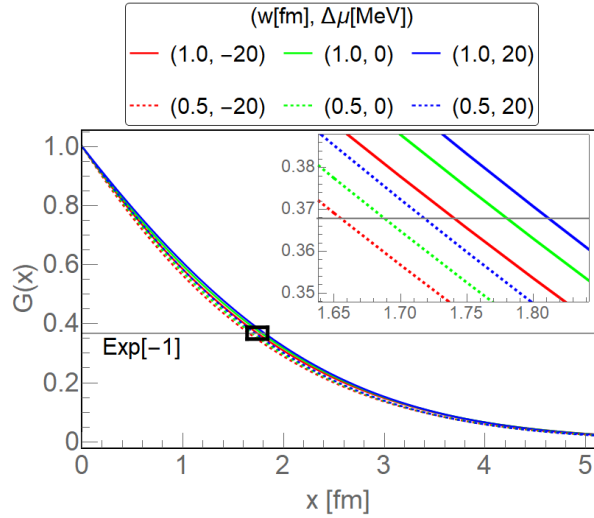


FIG. 5. The normalized nonlocal correlation $G(x)$ near the PT point. The legends are the same as that in Fig. 3. The inset is an enlargement of the cross region marked in the plot.

where x_p denotes the spatial location of the PT point. We plot the result in Fig. 5. The normalized nonlocal correlation doesn't exactly decay exponentially, so we determine the correlation length ξ by requiring $G(\xi) = \exp(-1)$. The ξ again smoothly increases from the crossover regime ($\Delta\mu < 0$) to the first order phase transition regime ($\Delta\mu > 0$), and decreases as

the increase of the temperature gradient. With the current parameter set, our estimation of the correlation length is $\xi \approx 1.74$ fm in the central part of the brick cell, which is significantly larger than $\xi \approx 1$ fm in the periphery.¹

VI. DISCUSSION

We have developed a method to figure out the stablest order parameter profile and the fluctuations in a temperature-nonuniform system. In different PT scenarios, both the fluctuations and the correlation length at the PT point are enhanced near the transition point, and decrease as the increase of temperature gradient. Especially, there is no critical behavior to identify the CP from the first order PT and crossover. By analyzing the temperature at the PT point of different $\Delta\mu$, we conclude that the PT temperature is approximately 7 MeV and 14 MeV ahead, with temperature gradient 20 MeV/fm and 40 MeV/fm, respectively. This means that if the effect of nonuniform temperature is the dominant factor, the hadrons will form before QGP cools to the equilibrium PT temperature during the fireball expansion. In addition, our studies on the correlation length show that ξ increases significantly at the PT point.

In the realistic fireball expansion, the temperature profile as well as the baryon chemical potential profile varies with the evolution of the QCD matter. Even in the Markov approximation, statistical average over fluctuations in different profiles is needed to figure out an effective dynamical PT line. We expect the statistical average will not change our results qualitatively. However, since the correlation length near the dynamical PT surface increases significantly in our calculation, the slowing down of dynamics is expected during PT in both the first order PT regime and crossover regime. The memory effect is enhanced and may not be neglectable, as is pointed in a couple of pioneer works [20, 37, 40–46]. A combination of the nonuniform temperature effects and the dynamical effects should provide a better description to the dynamical PT in the fireball expansion.

ACKNOWLEDGMENTS

This work was supported by the Research Council of Norway through its Centres of Excellence funding scheme (project no. 262633, “QuSpin”). Lijia Jiang thanks Xiaofeng Luo and Bao-Chi Fu for helpful discussions.

¹ Note that with a different parameter setting, $a = 0.22 \text{ fm}^{-2}$, $b = -0.1 \text{ fm}^{-1}$, and $c = 1.6$, the correlation length is $\xi \approx 1.5$ fm in the periphery and becomes 2.55 fm at the PT point. The amplitude of ξ is also about 1.7 times enhanced.

- [1] M. M. Aggarwal et al. (STAR), (2010), [arXiv:1007.2613 \[nucl-ex\]](#).
- [2] [BES-II White Paper \(STAR Note 2014\)](#).
- [3] W. Busza, K. Rajagopal, and W. van der Schee, *Annual Review of Nuclear and Particle Science* **68**, 339 (2018), <https://doi.org/10.1146/annurev-nucl-101917-020852>.

- [4] J. Adam *et al.* (STAR), (2020), [arXiv:2001.02852 \[nucl-ex\]](#).
- [5] M. Abdallah *et al.* (STAR), (2021), [arXiv:2101.12413 \[nucl-ex\]](#).
- [6] J. Letessier and J. Rafelski, [Hadrons and Quark–Gluon Plasma](#), Cambridge Monographs on Particle Physics, Nuclear Physics and Cosmology (Cambridge University Press, 2002).
- [7] Y. Aoki, G. Endrődi, Z. Fodor, S. D. Katz, and K. K. Szabó, *Nature* **443**, 675 (2006).
- [8] A. Bazavov *et al.* (HotQCD), *Phys. Rev. D* **85**, 054503 (2012).
- [9] K. Fukushima and C. Sasaki, *Progress in Particle and Nuclear Physics* **72**, 99 (2013).
- [10] A. Bzdak, S. Esumi, V. Koch, J. Liao, M. Stephanov, and N. Xu, *Physics Reports* **853**, 1 (2020).
- [11] L. Adamczyk *et al.* (STAR), *Phys. Rev. C* **96**, 044904 (2017).
- [12] B. Abelev *et al.* (ALICE Collaboration), *Phys. Rev. C* **88**, 044910 (2013).
- [13] B. Abelev *et al.* (ALICE Collaboration), *Phys. Rev. Lett.* **109**, 252301 (2012).
- [14] A. Andronic, P. Braun-Munzinger, K. Redlich, and J. Stachel, *Nature* **561**, 321 (2018).
- [15] X. Luo, S. Shi, N. Xu, and Y. Zhang, *Particles* **3**, 278 (2020).
- [16] K. Fukushima, B. Mohanty, and N. Xu, (2020), [arXiv:2009.03006 \[hep-ph\]](#).
- [17] A. Bazavov *et al.* (HotQCD), *Phys. Rev. D* **90**, 094503 (2014).
- [18] O. Kaczmarek, F. Karsch, E. Laermann, C. Miao, S. Mukherjee, P. Petreczky, C. Schmidt, W. Soeldner, and W. Unger, *Phys. Rev. D* **83**, 014504 (2011).
- [19] W.-j. Fu, X. Luo, J. M. Pawłowski, F. Rennecke, R. Wen, and S. Yin, (2021), [arXiv:2101.06035 \[hep-ph\]](#).
- [20] S. Mukherjee, R. Venugopalan, and Y. Yin, *Phys. Rev. C* **92**, 034912 (2015).
- [21] S. Mukherjee, R. Venugopalan, and Y. Yin, *Phys. Rev. Lett.* **117**, 222301 (2016).
- [22] L. Jiang, S. Wu, and H. Song, *Nucl. Phys. A* **967**, 441 (2017).
- [23] S. Wu, Z. Wu, and H. Song, *Phys. Rev. C* **99**, 064902 (2019).
- [24] P. Huovinen, P. Kolb, U. Heinz, P. Ruuskanen, and S. Voloshin, *Physics Letters B* **503**, 58 (2001).
- [25] M. Luzum and P. Romatschke, *Phys. Rev. C* **78**, 034915 (2008).
- [26] C. Gale, S. Jeon, B. Schenke, P. Tribedy, and R. Venugopalan, *Phys. Rev. Lett.* **110**, 012302 (2013).
- [27] H. Song and U. Heinz, *Phys. Rev. C* **77**, 064901 (2008).
- [28] L. Du and U. Heinz, *Computer Physics Communications* **251**, 107090 (2020).
- [29] C. Shen and S. Alzhrani, *Phys. Rev. C* **102**, 014909 (2020).
- [30] D.-U. Jungnickel and C. Wetterich, *Phys. Rev. D* **53**, 5142 (1996).
- [31] V. Skokov, B. Friman, E. Nakano, K. Redlich, and B.-J. Schaefer, *Phys. Rev. D* **82**, 034029 (2010).
- [32] C. D. Roberts and A. G. Williams, *Progress in Particle and Nuclear Physics* **33**, 477 (1994).
- [33] D. U. Jungnickel and C. Wetterich, *Phys. Rev. D* **53**, 5142 (1996).
- [34] B.-J. Schaefer and J. Wambach, *Phys. Part. Nucl.* **39**, 1025 (2008).
- [35] C. Nonaka and M. Asakawa, *Phys. Rev. C* **71**, 044904 (2005).
- [36] M. A. Stephanov, *Phys. Rev. Lett.* **107**, 052301 (2011).
- [37] L. Jiang, J.-H. Zheng, and H. Stoecker, (2017), [arXiv:1711.05339 \[nucl-th\]](#).
- [38] M. A. Stephanov, *Phys. Rev. Lett.* **102**, 032301 (2009).
- [39] L. Jiang, P. Li, and H. Song, *Phys. Rev. C* **94**, 024918 (2016).
- [40] C. Herold, M. Nahrgang, Y. Yan, and C. Kobdaj, *Phys. Rev. C* **93**, 021902 (2016).
- [41] M. Stephanov and Y. Yin, *Phys. Rev. D* **98**, 036006 (2018).
- [42] M. Nahrgang, M. Bluhm, T. Schäfer, and S. A. Bass, *Phys. Rev. D* **99**, 116015 (2019).
- [43] E. Shuryak and J. M. Torres-Rincon, *Phys. Rev. C* **100**, 024903 (2019).
- [44] K. Rajagopal, G. W. Ridgway, R. Weller, and Y. Yin, *Phys. Rev. D* **102**, 094025 (2020).
- [45] M. Bluhm *et al.*, *Nucl. Phys. A* **1003**, 122016 (2020).
- [46] L. Du, U. Heinz, K. Rajagopal, and Y. Yin, *Phys. Rev. C* **102**, 054911 (2020).